







Polaronic and Mott insulating phase of layered magnetic vanadium trihalide VCl_3 Dario Mastrippolito ^{1,*}, Luigi Camerano,¹ Hanna Świątek ^{2,3}, Břetislav Šmíd ⁴, Tomasz Klimczuk ^{2,3},
Luca Ottaviano ^{1,5} and Gianni Profeta ^{1,5}¹*Department of Physical and Chemical Sciences, University of L'Aquila, Via Vetoio, 67100 L'Aquila, Italy*²*Faculty of Applied Physics and Mathematics, Gdansk University of Technology, Narutowicza 11/12, 80-233 Gdansk, Poland*³*Advanced Materials Centre, Gdansk University of Technology, Narutowicza 11/12, 80-233 Gdansk, Poland*⁴*Faculty of Mathematics and Physics, Department of Surface and Plasma Science, Charles University, V Holešovičkách 2, 180 00 Prague 8, Czech Republic*⁵*CNR-SPIN L'Aquila, Via Vetoio, 67100 L'Aquila, Italy*

(Received 18 January 2023; revised 21 April 2023; accepted 14 June 2023; published 17 July 2023)

Two-dimensional (2D) van der Waals (vdW) magnetic $3d$ -transition metal trihalides are a new class of functional materials showing exotic physical properties useful for spintronic and memory storage applications. In this article, we report the synthesis and electromagnetic characterization of single-crystalline vanadium trichloride, VCl_3 , a novel 2D layered vdW Mott insulator, which has a rhombohedral structure ($R\bar{3}$, No. 148) at room temperature. VCl_3 undergoes a structural phase transition at 103 K and a subsequent antiferromagnetic transition at 21.8 K. Combining core levels and valence bands x-ray photoemission spectroscopy (XPS) with first-principles density functional theory (DFT) calculations, we demonstrate the Mott Hubbard insulating nature of VCl_3 and the existence of electron small 2D magnetic polarons localized on V atom sites by V-Cl bond relaxation. The polarons strongly affect the electromagnetic properties of VCl_3 promoting the occupation of dispersion-less spin-polarized V- $3d$ a_{1g} states and band inversion with e'_g states. Within the polaronic scenario, it is possible to reconcile different experimental evidences on vanadium trihalides, suggesting that also VI_3 hosts polarons. Our results highlight the complex physical behavior of this class of crystals determined by charge trapping, lattice distortions, correlation effects, mixed valence states, and magnetic states.

DOI: [10.1103/PhysRevB.108.045126](https://doi.org/10.1103/PhysRevB.108.045126)**I. INTRODUCTION**

Layered van der Waals (vdW) $3d$ -transition metal trihalides (MX_3 ; M = Cr, V; X = I, Br, Cl) crystals are nowadays considered for integration into spintronic and memory storage applications at nanoscale due to their intrinsic two-dimensional (2D) magnetism and exotic physical properties [1,2]. Although this class of compounds has particularly rich physics, currently, the research interest is moving toward the vanadium trihalides (VX_3) group, as they show higher magnetic transition temperatures than their Cr-based counterparts [3,4]. Vanadium tri-iodide, VI_3 , was recently studied by different experimental and theoretical approaches to disclosing the intricate nature of its electronic ground state, which is determined by the interplay between crystal field effects, spin-orbit coupling, and strong correlations [5–7]. Photoemission experiments [6,7] revealed VI_3 as a highly correlated Mott insulator with low-dispersing Hubbard bands that fall into the valence bands (VB), pointing out to an electronic ground state with occupied a_{1g} and half-filled e'_\pm doublet states [7]. However, until now, there has been no uniform consensus on the nature of its electronic structure nor on the other vanadium halides compounds. It should be to understand to which degree the members of the VX_3 family share the same physics or VI_3 represents a unique example. In this

article, we report the synthesis and characterization of a novel compound belonging to the vanadium trihalides class, namely, VCl_3 , accompanied by a thorough theoretical investigation via first-principles density functional theory (DFT) calculations in combination with photoemission experiments. Our results also provide a theoretical interpretation that explains contrasting experimental and theoretical evidence of VI_3 .

VCl_3 is predicted to be attractive for several applications since it has rich physics hosting quantum and valley Hall effects, high magnetoresistance, and skyrmions [8–11]. However, to date and to the best of our knowledge, only VI_3 and VBr_3 were successfully grown in the form of macroscopic single crystals [4,12], allowing for a complete physical characterization. On the other hand, VCl_3 has not yet been studied in its single-crystalline form and its electronic properties are still experimentally unexplored. VCl_3 has been predicted to be a metal [9,10,13–15], in contrast to the insulating behavior of the isostructural VI_3 , as well as a Mott insulator [16,17]. For these reasons, we have grown macroscopic single crystals of VCl_3 and investigated them by means of x-ray photoemission spectroscopy (XPS) to access electronic core levels and VB simultaneously and clarify its electronic nature. At variance with VI_3 and VBr_3 , which are usually grown by chemical vapor transport technique [4,12], we successfully grew single crystalline VCl_3 by the less common self-selecting vapor growth (SSVG) technique [18]. Details on the growth procedure are provided in the dedicated section in the Appendix. The SSVG technique is usually used for the growth of II-VI

*Corresponding author: dario.mastrippolito@graduate.univaq.it

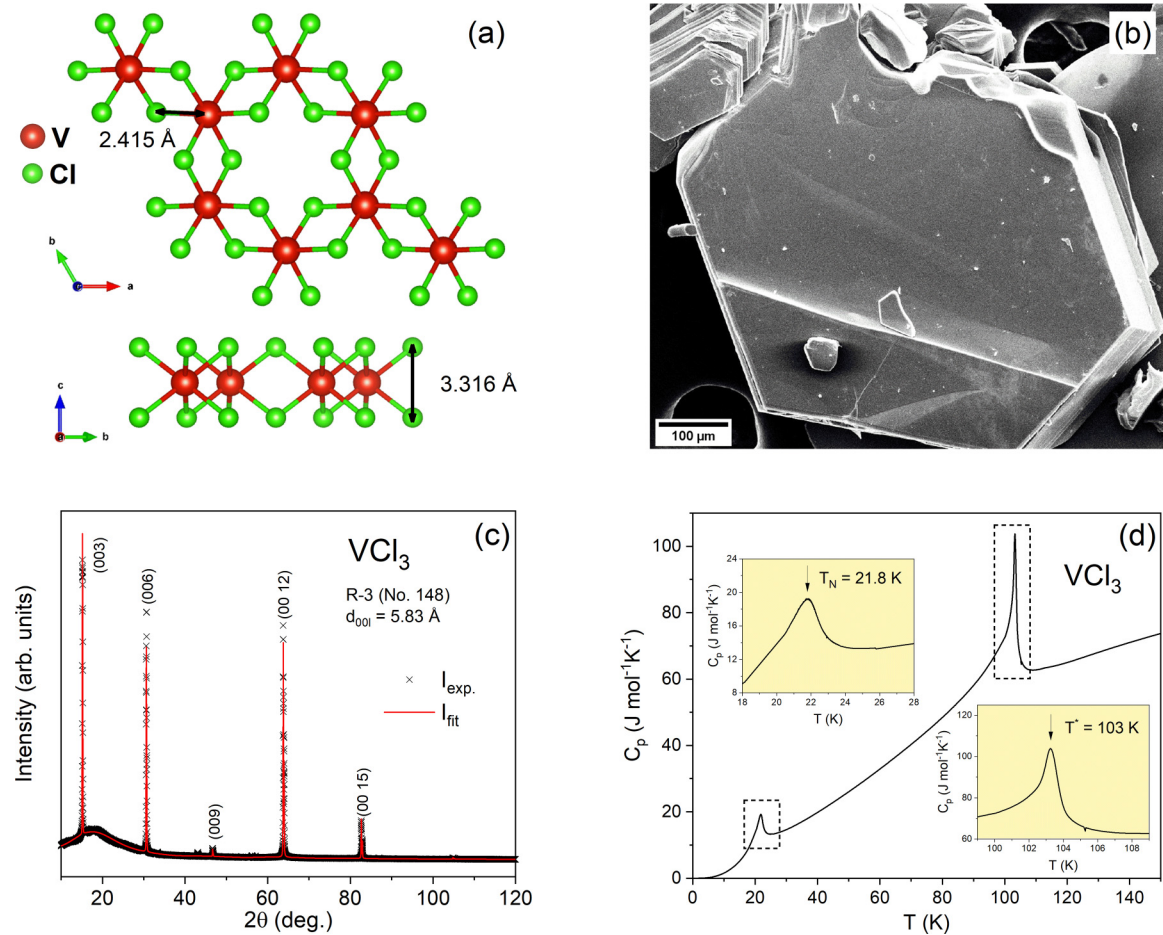


FIG. 1. (a) Top and side views of VCl_3 monolayer crystal structure. V and Cl atoms are represented in red and green spheres, respectively. (b) SEM image of VCl_3 flake-like crystals. (c) Room-temperature XRD experimental (black crosses) and $R\bar{3}$ -model fitted (red line) spectra of VCl_3 crystal. (d) Temperature-dependent heat capacity of VCl_3 crystal. Insets: the antiferromagnet phase transition at 21.8 K and the structural phase transition at 103 K.

and IV-VI semiconducting crystals, but more recently it also found application in the growth of some transition metal halides [19,20].

II. RESULTS AND DISCUSSION

We start our discussion by reporting the structural characterization of the as-grown crystals, which have a 3.0 ± 0.2 Cl/V atomic ratio double confirmed by energy-dispersive x-ray (EDX) analysis (see Fig. S1 [21]) and XPS. In its single-crystalline form, VCl_3 is a layered material having weak interlayer vdW interaction between each layer, whose thickness is 3.316 \AA [Fig. 1(a)] and is formed by a honeycomb lattice of V atoms bonded to two Cl sublayers. Vanadium atoms are octahedrally coordinated with Cl atoms with a bond length of 2.415 \AA . As is visible from the scanning electron microscopy (SEM) image of Fig. 1(b), the as-grown VCl_3 crystals have a form of plate-like hexagons with a size of $1.5 \times 1.5 \text{ mm}^2$ and a thickness of less than 0.1 mm. The crystals have a layered lamellar stacking that is easily exfoliable down to the 2D phase. In Fig. 1(c), we report the room-temperature x-ray diffraction (XRD) pattern of a single-crystalline VCl_3 . Only $00l$ reflections are detected

endorsing the layered phase of VCl_3 . For the LeBail profile refinement, we applied the rhombohedral BiI_3 -type structure ($R\bar{3}$, No. 148), which gives a layer spacing $d_{001} = 5.83 \text{ \AA}$ in good agreement with the one reported (5.78 \AA) in Ref. [22]. The temperature-dependent heat capacity measurements show that, upon cooling, VCl_3 undergoes a structural phase transition at $T^* = 103 \text{ K}$ and an antiferromagnetic transition at $T_N = 21.8 \text{ K}$ [Fig. 1(d)]. Those temperatures are consistent with the previously reported for polycrystalline VCl_3 [23,24].

Once the structure and the correct synthesis of the crystals have been ascertained, *in situ* mechanically exfoliated thin VCl_3 flakes were investigated by XPS [Fig. 2] for the analysis of the core levels (V- $2p$ and Cl- $2p$) and VB. The shape of the Cl- $2p$ core level spectrum is well described by a single Voigt doublet in contrast to the CrCl_3 case, where a Cl-vacancy-related component is clearly detected in Ref. [25]. The Cl- $2p$ doublet is centered at a binding energy (BE) of 198.1 eV , in agreement with the literature on VCl_3 powder [22], and has a spin-orbit (SO) splitting of 1.6 eV . The V- $2p$ core level has its main V- $2p_{3/2}$ component at a BE of 515.3 eV , as for the VCl_3 powder [22], and a SO splitting of 7.5 eV . The V- $2p$ is deconvoluted in three Voigt doublets revealing a multiplet structure that is ubiquitous in the MX_3 family [25–27]. The

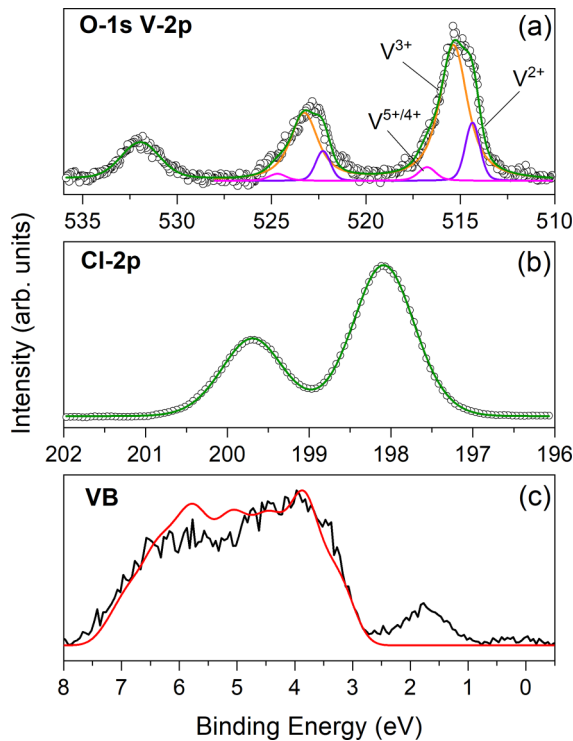


FIG. 2. XPS core levels and valence bands spectra of exfoliated VCl_3 flakes. The raw data (black), the cumulative fits (dark green), and the relative deconvolution (colored) are shown. (a) O-1s and V-2p core levels deconvolution. (b) Cl-2p core level deconvolution. (c) The experimental valence bands spectrum of VCl_3 flake (black) is directly compared to the DOS of pristine VCl_3 monolayer (red). The DOS is convoluted with a Gaussian function ($\sigma = 0.5$ eV) to account for the experimental broadening.

most dominant component at a BE of 515.3 eV, accounting for 81% of the total V-2p spectral area, is assigned to V^{3+} , fully consistent with the octahedral coordination of the V^{3+} with Cl^- ions. The second component at lower BE, 514.3 eV, weighs 15% of the total V-2p area and is assigned to V^{2+} , similar to what was observed in VI_3 [6,28]. The remaining 4% of the V-2p doublet at a BE of 516.8 eV, can be assigned to $\text{V}^{5+/4+}$ states [28,29]. Oxidation of the thin VCl_3 flakes is excluded by the analysis of the nearby O-1s core level, which is composed of one peak (centered at a BE of 531.9 eV) assigned to molecular O_2 and/or organics [29,30] reasonably originating from the underlying/surrounding carbon tape used as substrate (see the Appendix). Indeed, any O-1s signal from vanadium oxides is expected at a much lower BE around 530 eV [28,29]. The VB structure, reported in Fig. 2(c), shows an evident insulating phase. Indeed, the measured VB extends from 8 eV to about 3 eV BE, where we observe a net VB edge. Two main broad features are observed at 6 eV and 4 eV and a clearly resolved and localized peak is detected just above the VB at a BE of 1.7 eV.

To understand the nature of the measured VCl_3 electronic states, we carried out first-principles DFT + U calculations (see the Appendix for computational details). Both pristine VCl_3 monolayer and bulk cases were simulated but no substantial differences are found between the 2D and bulk phases (see Figs. S2, S3, and S4 [21]) and including spin-orbit cou-

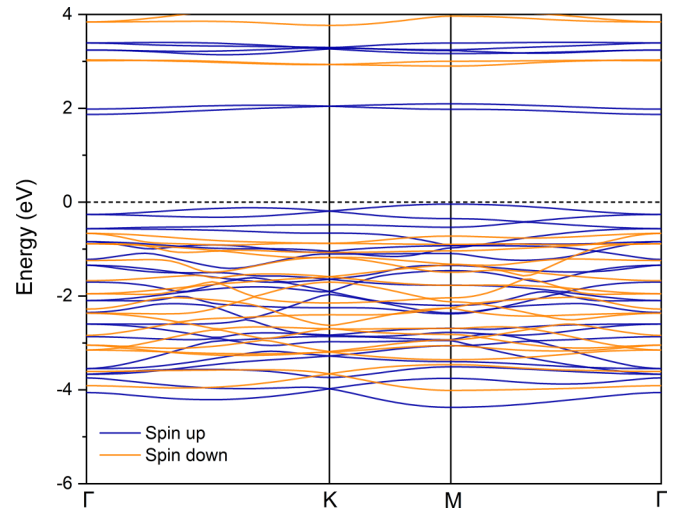


FIG. 3. Spin-resolved band structures of pristine VCl_3 monolayer.

pling (see Fig. S5 [21]) which is small and does not affect the resolution of the bands as for the other chlorine-based metal trihalide CrCl_3 [31]. The density of states with and without SOC are reported for comparison in Fig. S6 [21]. We find a ferromagnetic Mott insulating ground state for the VCl_3 monolayer, as for the CrCl_3 [25,32], whose VB states mainly originate from the hybridization between V-3d and Cl-3p states. The valence bands maximum (VBM) is constituted only of spin-up polarized states at the M point of the Brillouin zone resulting in an indirect band gap of 1.8 eV [Fig. 3]. However, the calculations of pristine VCl_3 are inconsistent with the reported XPS results. First, the predicted charge state of V atoms is V^{3+} , incompatible with the observed V^{2+} component in the V-2p core levels. Second, as evident in Fig. 2(c), the density of states (DOS) does not reproduce all features that emerge from the VB photoemission analysis. In fact, despite a satisfactory overall agreement in the BE region between 8 eV and 3 eV, the DOS does not predict any electronic states up to about 3 eV above the VBM, contrary to the experimental evidence. A critical inspection of the literature reveals that, indeed, these states were already detected also in other related systems, like VI_3 , even if not completely noticed or discussed but assigned to some spurious effects [6,7]. We think that their origin is still unclear and deserves a more careful theoretical explanation. As it will be demonstrated soon below, we attribute these states to the formation of polarons.

Polarons have been observed in several transition metal-based materials [33] and perovskite metal halides [34], but rarely in the 2D phase [35]. However, very recently, evidences of polaronic states were founded in layered chromium trihalides [36–39]. Polarons change radically the electronic properties, spin transport, and also magnetic phases. In extremely correlated Mott insulating ionic systems, like VCl_3 , even small perturbations in the electronic structure can lead, possibly, to the formation of polarons, which can be observed by XPS experiments and understood from the core levels and VB analysis [40–42]. In this regard, the observed V^{2+} core-level component leans towards the presence of an excess of electrons, whose origin could be ascribed to photoexcited core electrons [43], which remain trapped in the material, or

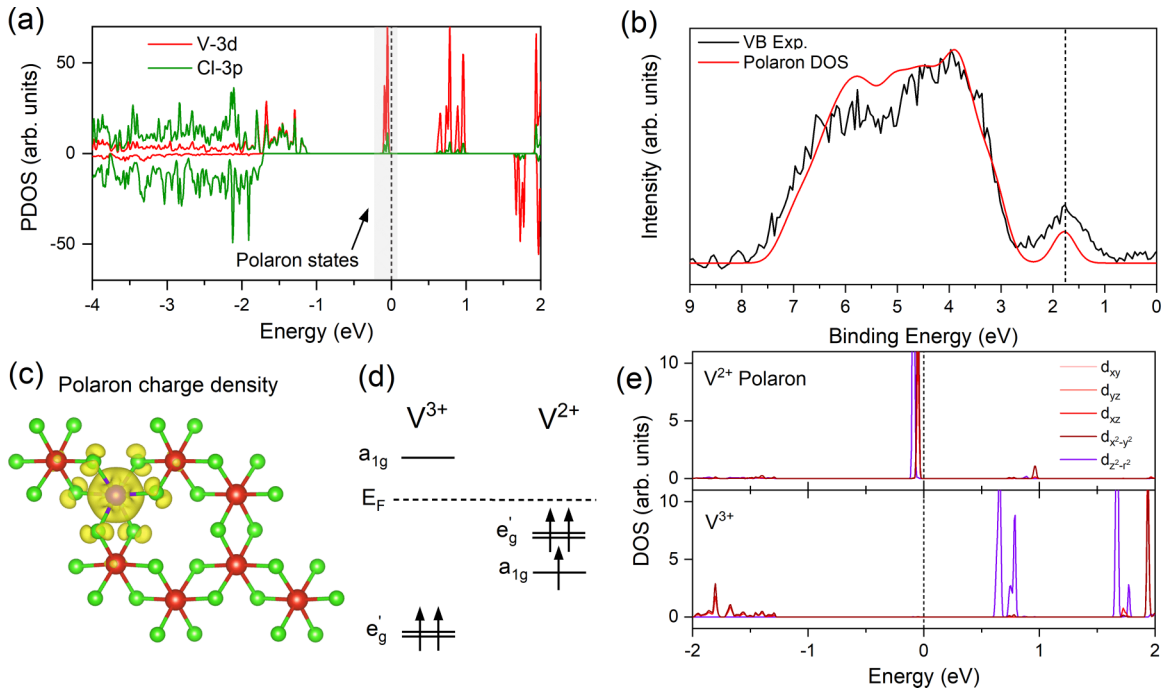


FIG. 4. Electron small 2D polarons of VCl_3 . (a) Spin-resolved partial DOS of polaronic 2×2 supercell of VCl_3 . Polaronic states are highlighted and contributed mainly by V-3d states. (b) The experimental valence bands spectrum of VCl_3 flake (black) is directly compared to the DOS of polaronic monolayer configurations (violet), convoluted with a Gaussian function ($\sigma = 0.5$ eV) to account for the experimental broadening. (c) Polaron charge density on the VCl_3 2×2 supercell. V and Cl atoms are represented in red and green spheres, respectively. (d) Electrons occupation for V^{3+} and V^{2+} polaronic configurations. (e) Spatially-projected DOS of V-3d states for V^{2+} polaronic atom and V^{3+} atom.

can be related to the presence of unstructured defects [33]. To validate this hypothesis we simulated a charged 2×2 supercell with one extra electron corresponding to the observed amount of V^{2+} signal. We find that the electron, driven by lattice distortions, localizes onto one of the eight V atom sites in the supercell, breaking the symmetry of the lattice and displacing the Cl atoms around the newly formed V^{2+} atom. By energy minimization calculations, we find that the formed electron polaron is energetically favored by 360 meV with respect to the corresponding symmetric electron-doped configuration in which all the vanadium atoms are equivalent and the electron equally delocalizes over the eight vanadium atoms. The trapped electron forms a small polaron in the relaxed VCl_6 octahedron structure resulting in a V-Cl bond length of 2.503 Å, enhanced by 4% with respect to the symmetric case [Figs. 4(c) and S6 [21]]. The structural perturbation induced by the excess electron is strongly localized around V^{2+} atom and extends up only to the second nearest-neighbor VCl_6 octahedrons surrounding the polaron. In the polaronic phase, some of the V-3d states, originating from the displaced V site, undergo a band crossing from the conduction to the valence bands, being occupied and localized within the band gap of VCl_3 [Fig. 4(a)]. It is interesting to note how the not-localized electronic configuration results in a metallic phase (see Fig. S6(a) [21]) and, thus, excludes it as a candidate to explain the photoemission spectra. As is clearly visible in Fig. 4(b), the direct comparison between the calculated DOS, obtained by the polaronic mechanism, and the experimental VB shows that now the experimental spectrum

is fully explained by the presence of an electronic polaron localized on a single V site. Specifically, the shape of the VB spectrum and the presence of the localized peak above the VB are predicted by our calculations with excellent accuracy both in energy position and relative intensity. Notably, the localized peak detected in the experimental VB is a direct fingerprint of the polaronic V-3d state. The presence of polarons has important implications for electronic occupations [Fig. 4(d)]. Indeed, in the undoped phase, the trigonal crystal field splitting of V^{3+} atom forces the occupation of the two-fold e'_g manifold in its ground state, while the a_{1g} state is unoccupied [44]. On the contrary, in the polaronic V^{2+} site, both e'_g and a_{1g} states are occupied, with inverted energy position. The a_{1g} state has a strong $d_{z^2-r^2}$ orientation and, thus, it produces a nonnegligible out-of-plane character of V-3d orbitals [Fig. 4(e)], which can profoundly alter the magnetic properties of VCl_3 . In addition, the value of the magnetic moment increases to $2.6 \mu_B$ for V^{2+} with respect to the undoped V^{3+} case which has a value of $1.9 \mu_B$. Besides, it is worth examining whether the polaronic state satisfies the criteria for its existence in the 2D phase, as proved in a recent article by Sio *et al.* in Eq. (9) of Ref. [35]. For this reason, we calculated the static ionic dielectric constant of VCl_3 ($\epsilon_{\text{ion}} = 0.98$) and derived the effective mass of the polaronic band ($m_* \simeq 3.7 m_e$). The values fully meet the existence requirements identifying the VCl_3 electron small polaron as a real 2D polaron.

Our discovery of magnetic polaron is not necessarily peculiar to the VCl_3 crystal but should be general and could exist also in other magnetic vdW materials hosting multiple valence atoms like vanadium and, in particular, in other VX_3

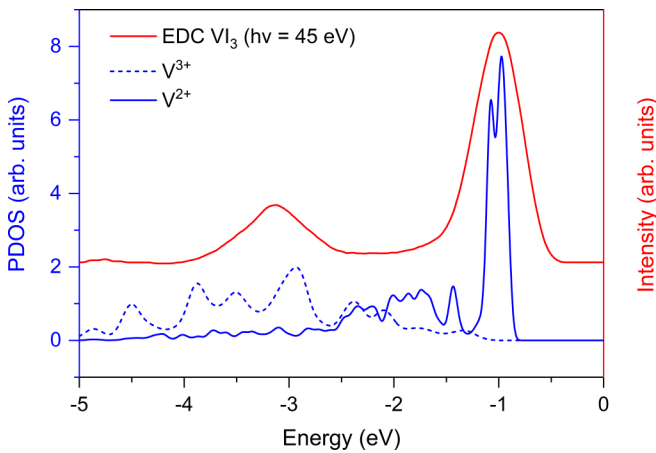


FIG. 5. Projected DOS for V-3d states for V^{2+} polaronic atom (blue) and V^{3+} atom (dashed blue) of VI_3 monolayer are compared with a VI_3 photoemission spectrum in resonance with V-3d states (red), which is adapted from Fig. 4(a) of Ref. [6].

compounds, such as VI_3 . As a confirmation of this, we will show below how the polaron formation naturally explains many recent (apparently contradicting) experiments on photoemission and x-ray magnetic circular dichroism (XMCD) [6,7,28,45]. Indeed, in Refs. [6,7,45], it was claimed that VI_3 has an occupied a_{1g} state. However, magnetic phases in VI_3 obtained by forcing the occupation of the a_{1g} orbital [5,45–47], which can explain the large orbital moment observed in Ref. [45], fail to predict the electronic valence band of VI_3 and its sharp peak around 1 eV below the Fermi level (see Refs. [6,7,28] and Fig. 5). To understand the origin of this anomalous sharp peak, in Ref. [6], the authors provided a tentative explanation proposing that the a_{1g} would be occupied by external electron doping (probably band bending, etc.), which will fill the a_{1g} state rigidly shifting the Fermi level. Apart from the exceptionally high electron concentration needed to completely fill one band, which is on the order of 10^{12} e/cm², this interpretation is disproved by the experiments of Bergner *et al.* [7] in which direct *n*-type doping on VI_3 was induced via alkaline deposition. Unexpectedly and at odds with respect to the interpretation of De Vita *et al.* [6], the authors did not observe a (rigid) band shift or relevant modifications in the VB caused by the electron doping, but only a progressive increase of the spectral weight of the localized V-3d states as a function of deposition time. Conversely, in our polaronic framework, all these experimental occurrences would be naturally explained by the formation of electron polarons. Indeed, we simulated the DOS of the VI_3 monolayer with the same procedure. In Fig. 5, we explicitly compare the VI_3 photoemission spectrum in resonance with V-3d states (adapted from Fig. 4(a) of Ref. [6]) with our projected DOS on different vanadium sites within our polaronic hypothesis. The peak near -1 eV can be only explained by the presence of a polaronic vanadium atom (V^{2+}), which is clearly missing otherwise. Our calculations predict that the polaron-induced structural distortion in VI_3 is similar to VCl_3 , i.e., the V-I bond increases by 0.7 Å to screen and accommodate the electron polaron charge. As further supporting evidence of the polaron formation in VI_3 , the V-2p core levels measured

in our VI_3 XPS experiments reported in Ref. [28] confirm the presence of both V^{3+} and V^{2+} components, which are compatible with the same polaronic scenario of VCl_3 . Within the polaronic context, the shoulder observed at the VI_3 VB edge [6,7,28] is now interpreted as a_{1g} polaronic states and the experiments of Bergner *et al.* [7] find an elegant explanation. Furthermore, the increasing population of the a_{1g} localized V-3d states by electron injection observed by Bergner *et al.* in VI_3 clearly indicates that V atoms continuously trap electrons eventually creating V^{2+} polarons. We verified this last occurrence also for VCl_3 simulating the VCl_3 DOS with an increasing polaronic concentration (see Fig. S7 [21]) and in fact, we observe a clear enhancement of the V-3d localized state intensity, without any modification of its binding energy.

III. CONCLUSION

In conclusion, our study provides the first experimental reference for the synthesis and characterization of the single-crystalline VCl_3 , accompanied by a combined experimental and theoretical understanding of its electronic nature. Photoemission experiments and first-principles DFT calculations clarify the Mott-Hubbard insulating behavior of the material and prove the existence of an extrinsic 2D polaronic phase, which determines the crossing of dispersion-less spin-polarized V-3d a_{1g} states from the conduction to the valence bands with a band inversion with e'_g states. The polaron picture not only well describes quantitatively the VCl_3 electronic structure but could offer a new key to explain the complex electromagnetic behavior and spin transport properties of the entire VX_3 crystal class, which is still debated. Our findings demonstrated that vanadium trihalides are a genuine case of 2D materials hosting real 2D magnetic polarons, and further enrich the appealing technological applications of this class of materials in the field of spintronics, memory storage, and quantum computing.

ACKNOWLEDGMENTS

We acknowledge P. Barone and M. Reticcioli for illuminating discussions in the early stage of the research and C. Tresca for his technical support. D.M. acknowledges the CERIC-ERIC Consortium for access to experimental facilities and financial support (proposal Grants No. 20222026 and No. 20227063). G.P. acknowledges support from CINECA Supercomputing Center through the IS CRA project and financial support from the Italian Ministry for Research and Education through the PRIN-2017 project “Tuning and understanding Quantum phases in 2D materials-Quantum 2D” (IT-MIUR Grant No. 2017Z8TS5B). This work was funded by the European Union-NextGenerationEU under the Italian Ministry of University and Research (MUR) National Innovation Ecosystem Grant No. ECS00000041 VITALITY-CUP E13C22001060006.

APPENDIX

1. Experimental Methods

High-quality single crystals of VCl_3 were obtained through re-crystallization of the commercially available polycrystalline VCl_3 (Sigma-Aldrich, 97% purity) through physical

vapor transport. The powder was weighed in an argon-filled glove box and then sealed in a silica tube with a diameter $D = 10$ mm and length $L = 180$ mm. The ampoule was placed in a horizontal tube furnace in a temperature gradient of 500–310° C and held there for a week, with the powder positioned in the hot zone. This method yielded flake-like VCl_3 crystals of size up to $1.5 \times 1.5 \times 0.1$ mm, grown on top of the polycrystalline powder at the source end of the ampoule. The size of the obtained single crystals was also found to strongly depend on the amount of the starting powder, with the best results obtained for smaller quantities of 200–250 mg. The growth followed the principles of the SSVG technique [18], in which crystals grow on the coolest part of the source powder which acts as a seed. SSVG requires very small temperature gradients; however, our preliminary attempt to recreate the crystal growth in a standard chamber furnace at 500° C, using only the natural horizontal temperature gradient, yielded crystals of unsatisfactory size. The as-grown VCl_3 crystals were sealed in silica tubes with a protected Ar atmosphere.

SEM measurements were carried out using a Zeiss Gemini SEM 500. An Oxford Instruments Ultim Max 100 detector was used for the EDX spectroscopy.

Determination of the crystal structure, as well as the orientation of the as-grown VCl_3 crystals, were done at room temperature by means of XRD using a Bruker D8 Phaser diffractometer equipped with a $\text{Cu K}\alpha$ radiation source and a LynxEye-XE detector. A single crystal plate was laid down on a zero-background Si holder and the XRD pattern was collected in the 2θ range from 10° to 120°. The XRD pattern of as-grown VCl_3 was processed by means of the LeBail refinement method using the TOPAS software.

The temperature dependence of heat capacity was measured using the Evercool II Quantum Design Physical Property Measurement System (PPMS). The measurements were conducted using the two- τ relaxation method, in the (1.9–300) K temperature range. The crystals were pressed to obtain a compact pellet and mounted on a sapphire plate using Apiezon H grease.

For the XPS investigation, VCl_3 crystals were mechanically exfoliated in a protected N_2 environment using the tape method [48]. The last piece of tape, loaded with thin VCl_3 flakes, was attached directly to carbon tape, which was used as sticky conductive substrate, and then inserted into the ultrahigh vacuum XPS setup. Finally, the tape was

peeled off *in situ* to have VCl_3 flakes with clean surfaces. XPS analysis was performed using a monochromatic $\text{Al-K}\alpha$ source ($h\nu = 1486.6$ eV) and a multichannel electron energy analyzer (Specs Phoibos 150). XPS data were recorded at room temperature. During preliminary XPS measurements, thick VCl_3 flakes exhibit massive charging effects upon x-ray flux exposure. To avoid charging of VCl_3 , the thick crystals were mechanically exfoliated many times to thin enough the VCl_3 flakes. The analysis of the core levels and valence bands was carried out after Shirley background subtraction and calibration to the C-1s core level binding energy set at a binding energy of 284.6 eV (C = C bond). Voigt functions were used to decompose the XPS core levels spectra.

2. Computational Methods

DFT calculations were performed using the Vienna *ab initio* Simulation Package (VASP) [49,50], within the generalized gradient approximation (GGA), and the Perdew-Burke-Ernzerhof (PBE) exchange-correlation functional [51]. Interactions between electrons and nuclei were described using the projector-augmented wave (PAW) method. Energy and force thresholds were set to 10^{-5} eV and 10^{-4} eVÅ⁻¹, respectively. A plane-wave kinetic energy cutoff of 450 eV was employed. The Brillouin zone (BZ) was sampled using $7 \times 7 \times 7$ Gamma-centered Monkhorst-Pack grids for the bulk phases, while a $12 \times 12 \times 1$ grid was used for the monolayer phase. To account for the on-site electron-electron correlation we used the GGA + U approach with an effective Hubbard term $U = 3.5$ eV consistent with the value calculated by He *et al.* [52] with linear response theory [53]. The van der Waals interactions between the VCl_3 layers were considered by adopting the DFT-D2 method [54]. The calculations for the bulk phase were carried out using the relaxed lattice parameters ($a = 6.084$ Å and $c = 17.625$ Å) with the spin-polarized PBE + U + vdW method (see Table S1 [21]). The monolayer phase was described in the supercell approach using a relaxed lattice parameter of $a = 6.084$ Å and a vacuum region of 15 Å.

The same approach was used for the DOS of VI_3 shown in Fig. 5. To account for the on-site electron-electron correlation we used the GGA + U approach with an effective Hubbard term $U = 3.7$ eV consistent with the value calculated by He *et al.* [52] with linear response theory [53]. The experimental bulk VI_3 lattice parameter was used in the calculations ($a = 6.93$ Å [55]).

- [1] C. Gong and X. Zhang, *Science* **363**, eaav4450 (2019).
- [2] D. L. Cortie, G. L. Causer, K. C. Rule, H. Fritzsche, W. Kreuzpaintner, and F. Klose, *Adv. Funct. Mater.* **30**, 1901414 (2020).
- [3] M. A. McGuire, *Crystals* **7**, 121 (2017).
- [4] T. Kong, K. Stolze, E. I. Timmons, J. Tao, D. Ni, S. Guo, Z. Yang, R. Prozorov, and R. J. Cava, *Adv. Mater.* **31**, 1808074 (2019).
- [5] K. Yang, F. Fan, H. Wang, D. I. Khomskii, and H. Wu, *Phys. Rev. B* **101**, 100402(R) (2020).
- [6] A. De Vita, T. T. P. Nguyen, R. Sant, G. M. Pierantozzi, D. Amoroso, C. Bigi, V. Polewczyk, G. Vinai, L. T. Nguyen, T. Kong *et al.*, *Nano Lett.* **22**, 7034 (2022).
- [7] D. Bergner, T. Kong, P. Ai, D. Eilbott, C. Fatuzzo, S. Ciocys, N. Dale, C. Stansbury, D. W. Latzke, E. Molina *et al.*, *Appl. Phys. Lett.* **121**, 183104 (2022).
- [8] Y. Li, Y. Liu, C. Wang, J. Wang, Y. Xu, and W. Duan, *Phys. Rev. B* **98**, 201407(R) (2018).
- [9] H. Liu, J.-T. Sun, M. Liu, and S. Meng, *J. Phys. Chem. Lett.* **9**, 6709 (2018).
- [10] Y. Feng, X. Wu, and G. Gao, *Appl. Phys. Lett.* **116**, 022402 (2020).
- [11] H. B. Tran and Y.-i. Matsushita, *arXiv:2209.02333*.
- [12] T. Kong, S. Guo, D. Ni, and R. J. Cava, *Phys. Rev. Mater.* **3**, 084419 (2019).
- [13] Y. Zhou, H. Lu, X. Zu, and F. Gao, *Sci. Rep.* **6**, 19407 (2016).

- [14] D. Zhao, M. Wei, F. Yang, W.-X. Ji, J. Lu, Y.-J. Zeng, and X. Yang, *Surf. Interfaces* **33**, 102293 (2022).
- [15] C. Ouettar, H. Yahi, K. Zanat, and H. Chibani, *Phys. Scr.* **98**, 025814 (2023).
- [16] S. Tomar, B. Ghosh, S. Mardanya, P. Rastogi, B. Bhadoria, Y. S. Chauhan, A. Agarwal, and S. Bhowmick, *J. Magn. Magn. Mater.* **489**, 165384 (2019).
- [17] S. Zhao, W. Wan, Y. Ge, and Y. Liu, *Ann. Phys. (Leipzig)* **533**, 2100064 (2021).
- [18] A. Szczerbakow and K. Durose, *Prog. Cryst. Growth Charact. Mater.* **51**, 81 (2005).
- [19] S. Kazim, M. Ali, S. Palleschi, G. D'Olimpio, D. Mastrippolito, A. Politano, R. Gunnella, A. Di Cicco, M. Renzelli, G. Moccia, O. A. Cacioppo, R. Alfonsetti, J. Strychalska-Nowak, T. Klimczuk, R. J. Cava, and L. Ottaviano, *Nanotechnology* **31**, 395706 (2020).
- [20] J.-Q. Yan and M. McGuire, *Phys. Rev. Mater.* **7**, 013401 (2023).
- [21] See Supplemental Material at <http://link.aps.org/supplemental/10.1103/PhysRevB.108.045126> for the EDX characterization (Fig. S1); optimized VCl_3 lattice parameters (Tab. S1); DOS for monolayer and bulk VCl_3 phases (Fig. S2); spin-resolved DOS of monolayer VCl_3 phase (Fig. S3); spin-resolved DOS of bulk VCl_3 phase (Fig. S4); DOS with/without spin-orbit coupling (Fig. S5); DOS and crystal structures of electron-doped and polaron configurations (Fig. S6); comparison of experimental valence bands and DOS at different polaron concentrations (Fig. S7); band structure and DOS of the VCl_3 unit cell in the polaronic phase (Fig. S8).
- [22] W. Klemm and E. Krose, *Z. Anorg. Chem.* **253**, 218 (1947).
- [23] C. Starr, F. Bitter, and A. Kaufmann, *Phys. Rev.* **58**, 977 (1940).
- [24] M. Kratochvílová, P. Doležal, D. Hovančík, J. Pospíšil, A. Bendová, M. Dušek, V. Holý, and V. Sechovský, *J. Phys.: Condens. Matter* **34**, 294007 (2022).
- [25] D. Mastrippolito, L. Ottaviano, J. Wang, J. Yang, F. Gao, M. Ali, G. D'Olimpio, S. Palleschi, A. Politano, S. Kazim, R. Gunnella, A. Di Cicco, A. Sgarlata, J. Strychalska-Nowak, T. Klimczuk, R. J. Cava, L. Lozzi, and G. Profeta, *Nanoscale Adv.* **3**, 4756 (2021).
- [26] M. Okusawa, K. Tsutsumi, T. Ishii, and T. Sagawa, *J. Phys. Soc. Jpn.* **51**, 510 (1982).
- [27] S. Kazim, D. Mastrippolito, P. Moras, M. Jugovac, T. Klimczuk, M. Ali, L. Ottaviano, and R. Gunnella, *Phys. Chem. Chem. Phys.* **25**, 3806 (2023).
- [28] D. Mastrippolito, H. Swiatek, P. Moras, M. Jugovac, R. Gunnella, L. Lozzi, P. Benassi, T. Klimczuk, and L. Ottaviano, *J. Lumin.* **251**, 119137 (2022).
- [29] G. Silversmit, D. Depla, H. Poelman, G. B. Marin, and R. De Gryse, *J. Electron Spectrosc. Relat. Phenom.* **135**, 167 (2004).
- [30] B. Payne, M. Biesinger, and N. McIntyre, *J. Electron Spectrosc. Relat. Phenom.* **184**, 29 (2011).
- [31] F. Xue, Y. Hou, Z. Wang, and R. Wu, *Phys. Rev. B* **100**, 224429 (2019).
- [32] D. Mastrippolito, J. Wang, G. Profeta, and L. Ottaviano, *J. Phys. Mater.* **5**, 014004 (2022).
- [33] C. Franchini, M. Reticcioli, M. Setvin, and U. Diebold, *Nat. Rev. Mater.* **6**, 560 (2021).
- [34] G. Kaur and H. N. Ghosh, *J. Phys. Chem. Lett.* **11**, 8765 (2020).
- [35] W. H. Sio and F. Giustino, *Nat. Phys.* **19**, 629 (2023).
- [36] X. Li, A. Wang, H. Chen, W. Tao, Z. Chen, C. Zhang, Y. Li, Y. Zhang, H. Shang, Y.-X. Weng *et al.*, *Nano Lett.* **22**, 8755 (2022).
- [37] W. Jin, H. H. Kim, Z. Ye, G. Ye, L. Rojas, X. Luo, B. Yang, F. Yin, J. S. A. Horng, S. Tian *et al.*, *Nat. Commun.* **11**, 4780 (2020).
- [38] D. Soriano and M. I. Katsnelson, *Phys. Rev. B* **101**, 041402(R) (2020).
- [39] T. Yin, J.-Y. You, Y. Huang, H. T. Thu Do, M. A. Prosnikov, W. Zhao, M. Serra, P. C. Christianen, Z. Sofer, H. Sun *et al.*, *Nano Lett.* **22**, 7784 (2022).
- [40] C. Chen, J. Avila, E. Frantzeskakis, A. Levy, and M. C. Asensio, *Nat. Commun.* **6**, 8585 (2015).
- [41] M. Kang, S. W. Jung, W. J. Shin, Y. Sohn, S. H. Ryu, T. K. Kim, M. Hoesch, and K. S. Kim, *Nat. Mater.* **17**, 676 (2018).
- [42] J. Casanova-Chafer, P. Umek, S. Acosta, C. Bittencourt, and E. Llobet, *ACS Appl. Mater. Interfaces* **13**, 40909 (2021).
- [43] S. Gridin, R. Williams, A. Belsky, E. Galenin, A. Gektin, N. Shiran, S. Vasiukov, and A. Vasil'ev, *J. Phys. Chem. C* **123**, 13519 (2019).
- [44] A. B. Georgescu, A. J. Millis, and J. M. Rondinelli, *Phys. Rev. B* **105**, 245153 (2022).
- [45] D. Hovančík, J. Pospíšil, K. Carva, V. Sechovsky, and C. Piamonteze, *Nano Lett.* **23**, 1175 (2023).
- [46] C. Huang, F. Wu, S. Yu, P. Jena, and E. Kan, *Phys. Chem. Chem. Phys.* **22**, 512 (2020).
- [47] L. M. Sandratskii and K. Carva, *Phys. Rev. B* **103**, 214451 (2021).
- [48] K. S. Novoselov, *Rev. Mod. Phys.* **83**, 837 (2011).
- [49] G. Kresse and J. Hafner, *Phys. Rev. B* **47**, 558 (1993).
- [50] G. Kresse and D. Joubert, *Phys. Rev. B* **59**, 1758 (1999).
- [51] J. P. Perdew, K. Burke, and M. Ernzerhof, *Phys. Rev. Lett.* **77**, 3865 (1996).
- [52] J. He, S. Ma, P. Lyu, and P. Nachtigall, *J. Mater. Chem. C* **4**, 2518 (2016).
- [53] M. Cococcioni and S. de Gironcoli, *Phys. Rev. B* **71**, 035105 (2005).
- [54] S. Grimme, J. Antony, S. Ehrlich, and H. Krieg, *J. Chem. Phys.* **132**, 154104 (2010).
- [55] T. Marchandier, N. Dubouis, F. Fauth, M. Avdeev, A. Grimaud, J.-M. Tarascon, and G. Rousse, *Phys. Rev. B* **104**, 014105 (2021).